Check for updates

OPEN

Room temperature and high response ethanol sensor based on two dimensional hybrid nanostructures of WS$_2$/GONRs

Hassan Ahmadvand[1], Azam Iraji zad[1,2]✉, Raheleh Mohammadpour[1]✉, Seyed Hossein Hosseini-Shokouh[3] & Elham Asadian[4]

Here in this research, room temperature ethanol and humidity sensors were prepared based on two dimensional (2D) hybrid nanostructures of tungsten di-sulfide (WS$_2$) nanosheets and graphene oxide nanoribbons (GONRs) as GOWS. The characterization results based on scanning electron microscopy (SEM), energy dispersive X-ray spectroscopy (ESD), Raman spectroscopy and X-ray diffraction (XRD) analysis confirmed the hybrid formations. Ethanol sensing of drop-casted GOWS films on SiO$_2$ substrate indicated increasing in gas response up to 5 and 55 times higher compared to pristine GONRs and WS$_2$ films respectively. The sensing performance of GOWS hybrid nanostructures was investigated in different concentrations of WS$_2$, and the highest response was about 126.5 at 1 ppm of ethanol in 40% relative humidity (R.H.) for WS$_2$/GONRs molar ratio of 10. Flexibility of GOWS was studied on Kapton substrate with bending radius of 1 cm, and the gas response decreased less than 10% after 30th bending cycles. The high response and flexibility of the sensors inspired that GOWS are promising materials for fabrication of wearable gas sensing devices.

Ethanol is one of the most widespread consumable volatile organic compounds in today's industries, medicine, foods, drug and biological applications. Long-term exposure cause irritation of the nose and throat, nausea, fatigue, loss of coordination, damage to the liver, kidneys, and central nervous system, and can cause cancer[1–4]. So, reliable portable room temperature ethanol sensors with a fast and reversible response, along with low cost and low power consumption play significant roles in human health and environmental monitoring. Nowadays, detection of low concentration of harmful gases seems promising through preparation gas sensors based on new 2D nanostructures like transition metal di-chalcogenides layered materials (TMDCs)[5–9]. TMDCs have the general formula MX$_2$, where M is a transition metal such as tungsten, and X is a chalcogenide element such as sulfur[10]. They have presented suitable properties to fabricate fast and reversible gas sensor devices due to large surface areas, active edges, availability of surface defects, or vacancies for gas molecules physisorption. Although fast charge transfer process between absorbed molecules and surface of TMDCs speeds up the sensing performance, weak connections between the flakes may cause fluctuating behavior and high electrical resistance and reduce gas response values[11]. Therefore hybrid formations based on relative conductive media and TMDCs can improve stability and gas response as was suggested by Park et al. on rGO/MoS$_2$ humidity sensors[12]. Herein, room temperature and flexible resistive ethanol sensors were prepared based on 2D hybrid nanostructures of graphene oxide nanoribbons (GONRs) and WS$_2$ nanosheets (as GOWS) by a simple drop-casting method. WS$_2$, as one of the most operational and stable members of TMDCs family[13], is an intrinsic n-type semiconductor with a hexagonal layered structure that its sheets are held together by van der Waals interaction and each layer consists of a slab S–W–S sandwich[14]. GONRs are excellent active and conductive media for gas sensing because of large dangling bonds around the edges and surface functional groups[15,16]. WS$_2$ nanosheets were synthesized by chemical vapor transport (CVT) method[17,18] and GONRs were prepared by unzipping of multi-wall Carbon

[1]Institute for Nanoscience and Nanotechnology, Sharif University of Technology, 14588 Tehran, Iran. [2]Department of Physics, Sharif University of Technology, 14588 Tehran, Iran. [3]School of Metallurgy and Materials Engineering, College of Engineering, University of Tehran, Tehran, Iran. [4]Department of Medical Physics and Biomedical Engineering, School of Medicine, Shahid Beheshti University of Medical Sciences, Tehran, Iran. ✉email: iraji@sharif.edu; mohammadpour@sharif.edu
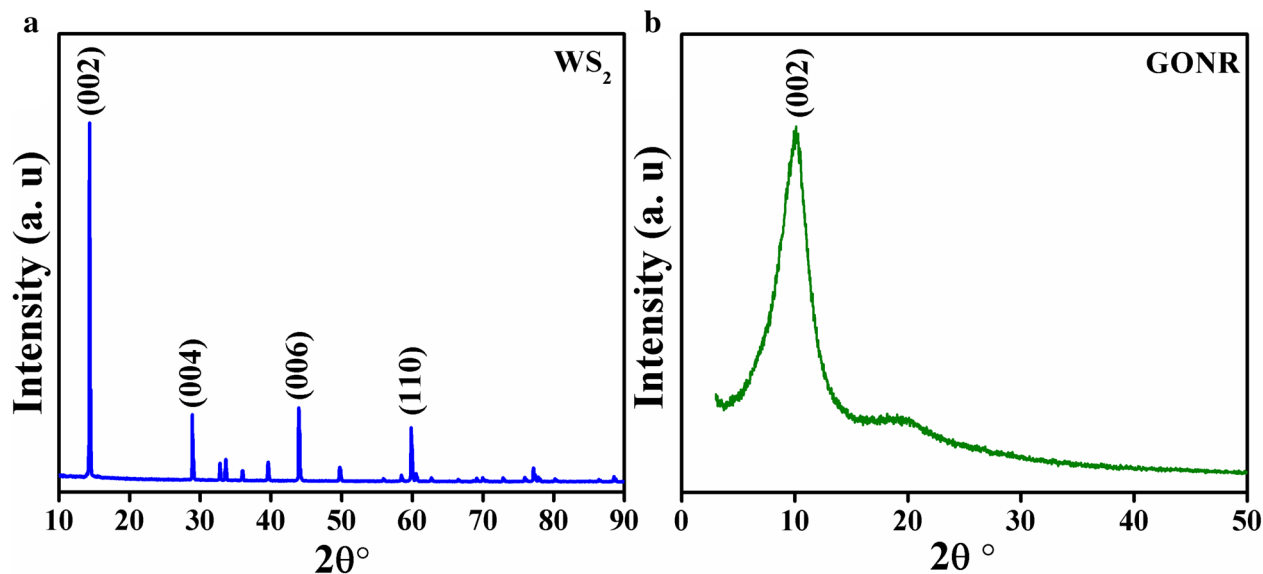
Figure 1. XRD spectra for CVT synthesized WS$_2$ (**a**), and GONRs (**b**).

nanotubes (MWCNTs) as reported by Tour's group with slight modifications[19], respectively. GOWSs were prepared in a simple way, the solutions contain of WS$_2$ nanosheets and GONRs were mixed with a magnetic stirrer and sonicated at room temperature. Gas sensing properties of GOWS samples were investigated for ethanol vapor and humidity at room temperature (about 25 °C ± 2 °C,) with different molar ratio of WS$_2$/GONRs, on SiO$_2$ substrate. Morphological and structural analysis of the as-prepared samples were performed using SEM, EDS, and Raman spectroscopy which verified the formation of heterojunction structures between WS$_2$ and GONRs. To study the effects of WS$_2$ concentration on the gas sensing properties of GOWS, the molar ratio of WS$_2$/GONRs (= X) was set to different values and the samples were named as GOWSX with X = 1, 5, 10,15and 20. The heterojunction formations in GOWS samples presented considerable higher and less fluctuating responses. The results on Kapton substrate indicated that GOWS is a competitive material to fabricate flexible and wearable gas sensors.

Results and discussion

The synthesized materials were subjected to X-ray powder diffraction analysis (XRD) via a Philips X'pert instrument operating with Cu K$_\alpha$ radiation (λ = 1.54 Å) at 40 kV/40 mA diffractometer. The characteristic peaks of WS$_2$ and GONRs are appeared in the XRD results as shown in Fig. 1a,b and are in good agreement with those of previous reports[14,20]. Surface morphology and structure of the prepared materials were characterized by means of scanning electron microscope (SEM) and energy dispersive X-ray spectroscopy (EDS) maps. Our microscopic observations showed a uniform dispersion of WS$_2$ flakes between nanoribbons in GOWS samples. The SEM image of an attached hexagonal WS$_2$ flack with wrinkled GONRs is shown in Fig. 2a. To verify their composition, EDS maps were carried on the sample (Fig. 2b). The elemental distribution images of oxygen, tungsten, carbon, and sulphur are demonstrated in Fig. 2c–f, respectively which indicate the successful formation of WS$_2$/GONRs heterojunctions in the prepared samples.

In the following, Raman spectroscopy was performed via a Raman spectrometer equipped with an Nd-YAG laser (λ = 532 nm), with a spectral resolution of 1 cm^{-1} (Teksan Raman microscope). The Raman scatterings of GOWS10 and GOWS20 films in comparison to pristine WS$_2$ and GONRs are displayed in Fig. 3a,b. The vibrational E$_{2g}$ and A$_{1g}$ modes that are attributed to in-plane and out-of-plane vibrations were appeared at 345.5 cm^{-1} and 416.3 cm^{-1} for pristine WS$_2$, respectively[21]. In GOWS20 and GOWS10 samples Raman shifts were observed in E$_{2g}$ from 348.5 to 338.5 and 341.5 cm^{-1}, and A$_{1g}$ from 416.3 to 410 and 341.5 cm^{-1}, respectively. The characteristic D-band and G-band of GONRs[22] appeared at 1,360 cm^{-1} and 1,600 cm^{-1}, respectively, while the Raman data showed in Fig. 3b represented similar shifts. Therefore the SEM and EDS observations and the shifts in the Raman spectra are evidences for appropriate heterojunctions between WS$_2$ and GONRs.

Gas sensing results. The sensors were fabricated by drop-casting of equal volume of GOWSs samples, pristine GONRs, and pristine WS$_2$ solutions on a SiO$_2$ substrate, including sputtered gold interdigitated electrodes with an interspacing of 100 μm and an active area of 10 mm × 10 mm. Ethanol sensing properties of the samples were measured in a breath simulator setup at room temperature. Dynamic gas sensing curves for 7, 9 and 11 ppm of ethanol in a mixture of air with about 40% R.H. were obtained at room temperature and the results are depicted in Fig. 4a. Electrical resistance for WS$_2$, GOWS10, and GONRs samples in air was measured about 10 MΩ, 1 MΩ, and 100 KΩ, respectively. The response of the sensors is defined by (I—I$_0$)/I$_0$ where I$_0$ refers to the electrical sensor current in air and I represents the electrical current in the presence of target gas.

GONRs sample indicated higher response and longer rise and recovery times than those of WS$_2$, as expected for wrinkle layered structures. Interestingly, the formation of WS$_2$/GONRs heterojunctions in GOWS samples
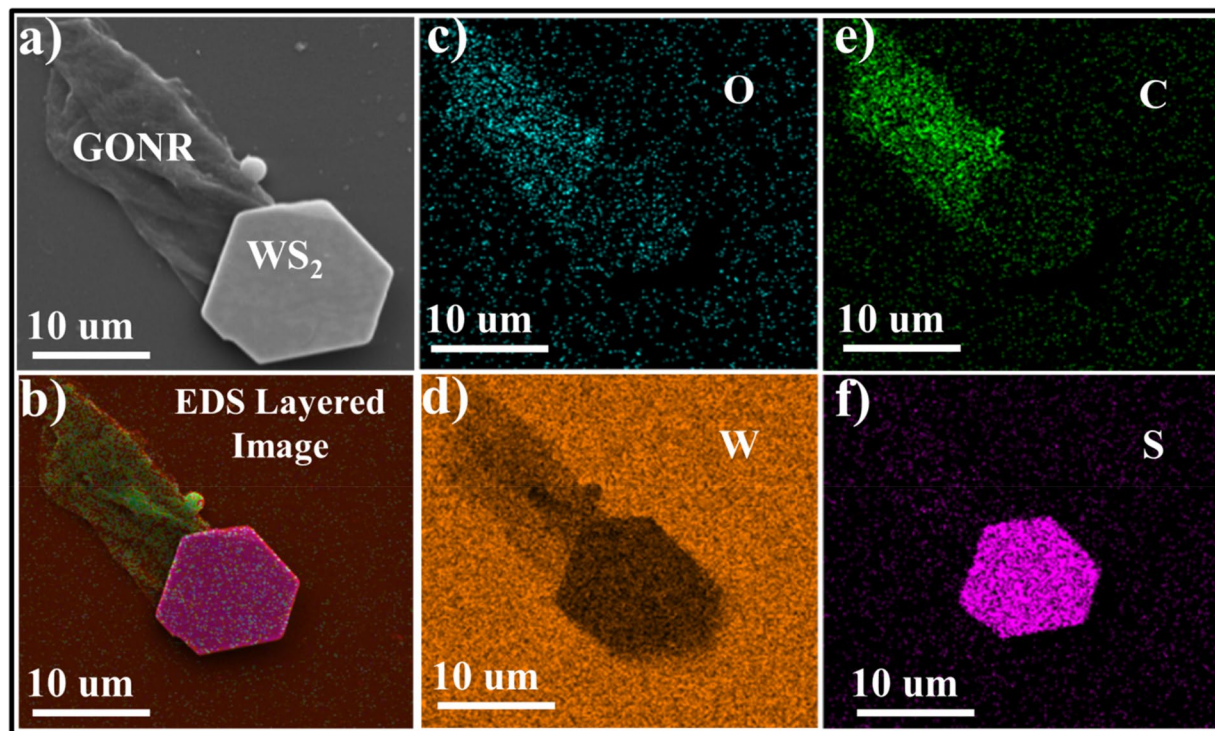
Figure 2. SEM image (**a**), and EDS layered image (**b**) of an attached hexagonal WS$_2$ flack with wrinkled GONRs. Elemental map of oxygen (**c**), tungsten (**d**), carbon (**e**), sulfur (**f**), in GOWS.
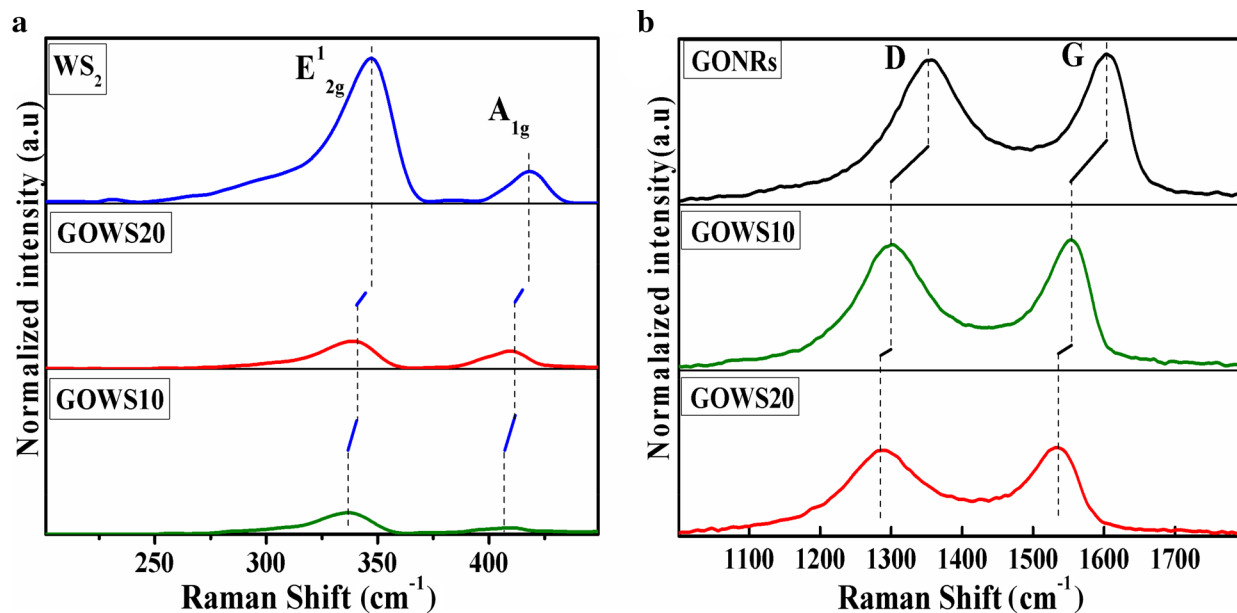

Figure 3. Raman spectra of pristine WS$_2$ (**a**) and GONRs (**b**) compared with those of GOWS10 and GOWS20.

resulted in considerable enhancement in the response values for various ethanol concentrations. In fact, graphene oxide nanoribbons enhanced electrical connectivity of the gas sensitive WS$_2$ flakes and resulted in a higher and less fluctuating electrical current in GOWS samples. The dynamic curves show two different trends; the fast one is related to charge transfer via water-water and water–ethanol hydrogen-bonding networks, while the slow process is due to the permeation of gas molecules into the inter-layers of GONRs. Figure 4b shows the initial rise in the response curves of GONRs, GOWS10 and GOWS20 at 5 ppm of ethanol@40% R.H. It is rational that sample with higher WS$_2$ contents has faster response. Figure 5a displays the response values for all samples toward 40% R.H. and 5, 11, 15 and 21 ppm of ethanol. The results show that GOWS10 have the maximum gas response value compared to others. The response of GONRs, WS$_2$ and GOWS10 are presented in Fig. 5b as the function of ethanol concentrations from 1 to 21 ppm in a mixture of 40% R.H.
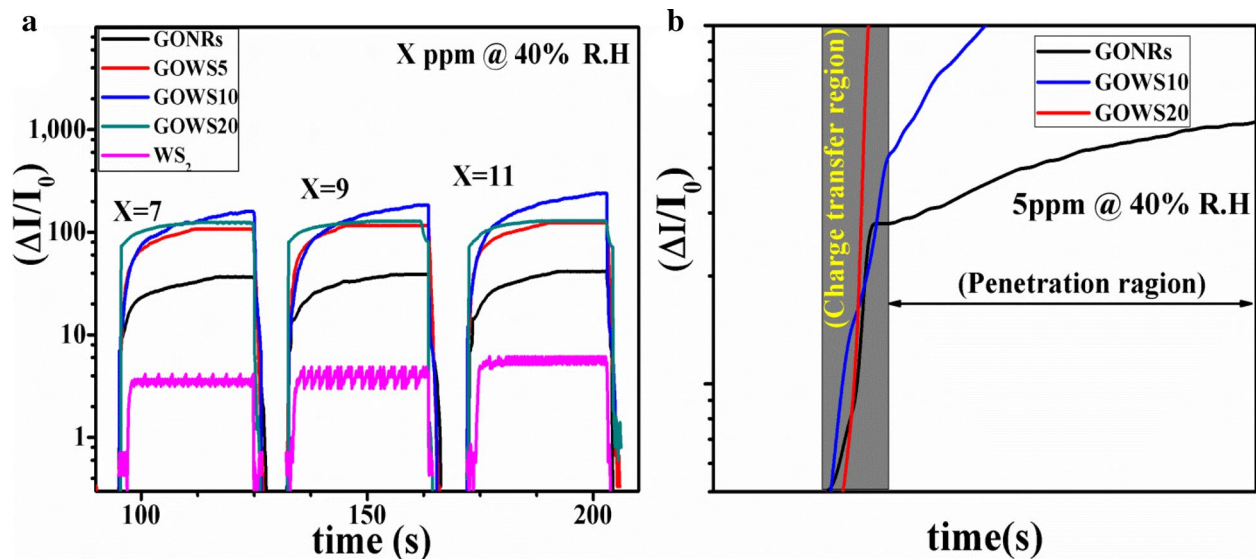
Figure 4. Dynamic response curves of pristine WS_2, GOWS5, GOWS10, GOWS20 and pristine GONRs for 40% humidity, 7, 9 and 11 ppm of ethanol at room temperature (**a**), an initial rise in response curves for GONRs, GOWS10 and GOWS20 at 5 ppm of ethanol@40% R.H. (**b**).
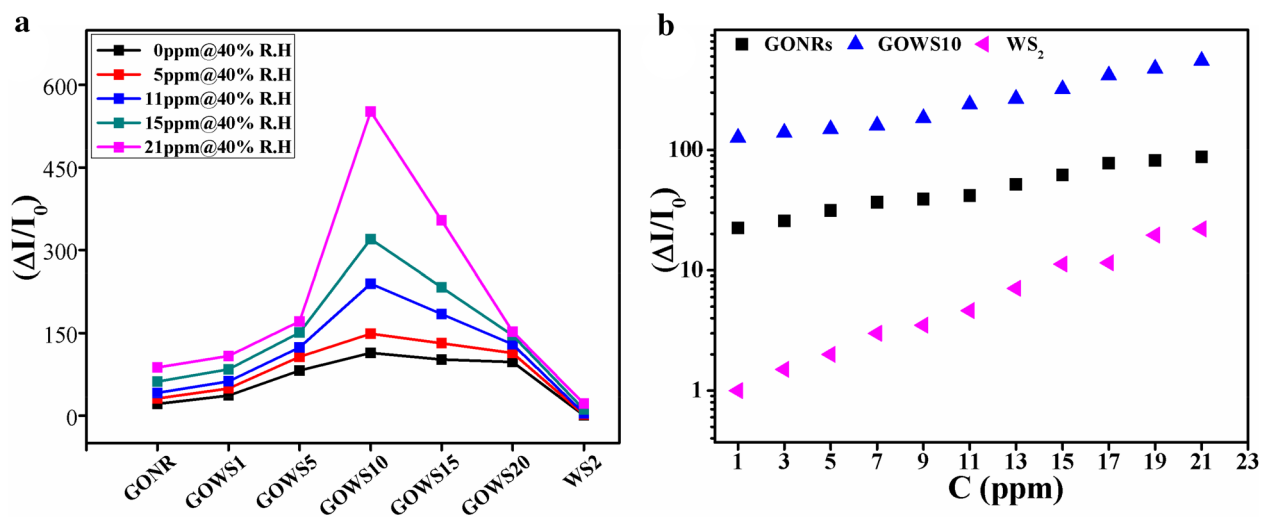

Figure 5. Response values for all samples toward 40% R.H. and 5, 11, 15 and 21 ppm of ethanol (**a**), response values of GONRs, WS_2 and GOWS10, as a function of ethanol concentrations in a mixture of air with about 40% R.H. (**b**).

Two mechanisms have considered for gas sensing; one the hydrogen bond networks formation and the other charge transfer. It is well-known that 2D layered structures of WS_2 provide high surface sites, such as dangling bonds at the edges, defects and sulfur vacancies, as well as oxygen active sites for physisorption of near-surface molecules[23]. Hence ethanol response could be attributed to charge transfer mechanism[24] between physisorbed molecules and the active sites. According to previous studies based on density functional theory (DFT) calculations, the physically absorbed ethanol molecules act as electron donor[25,26] and as result, decrease the electrical resistance of n-type WS_2. The adsorption energy of the gas molecules is defined by $E_{(ads)} = E_{(total)} - E_{(WS2)} - E_{(gas)}$, where $E_{(total)}$, $E_{(WS2)}$, and $E_{(gas)}$ refer to total energy of the system after gas adsorption on WS_2, the energy of WS_2, and the energy of gas molecules, respectively. In general, the charge transfer mechanism could be explained as follows:

$$C_2H_5OH_{(gas)} + V_{(on\ surface)} \rightarrow C_2H_5OH_{(ads)} + ne^-$$
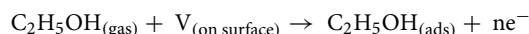
where $V_{(on\ surface)}$ is the WS_2 surface vacancies. Upon exposure, the ethanol molecule with low electron affinity serves as electron donor, and transfers its electrons to the conduction band of n-type WS_2, thus increased electrical conductivity; however, the details in this process are still lack. In addition, humidity response is related to physisorption on the surface active sites and formation of water–water hydrogen bond networks that causes proton hopping as explained in Grotthuss model [27–29]. Consequently, the network enhances charge transport via
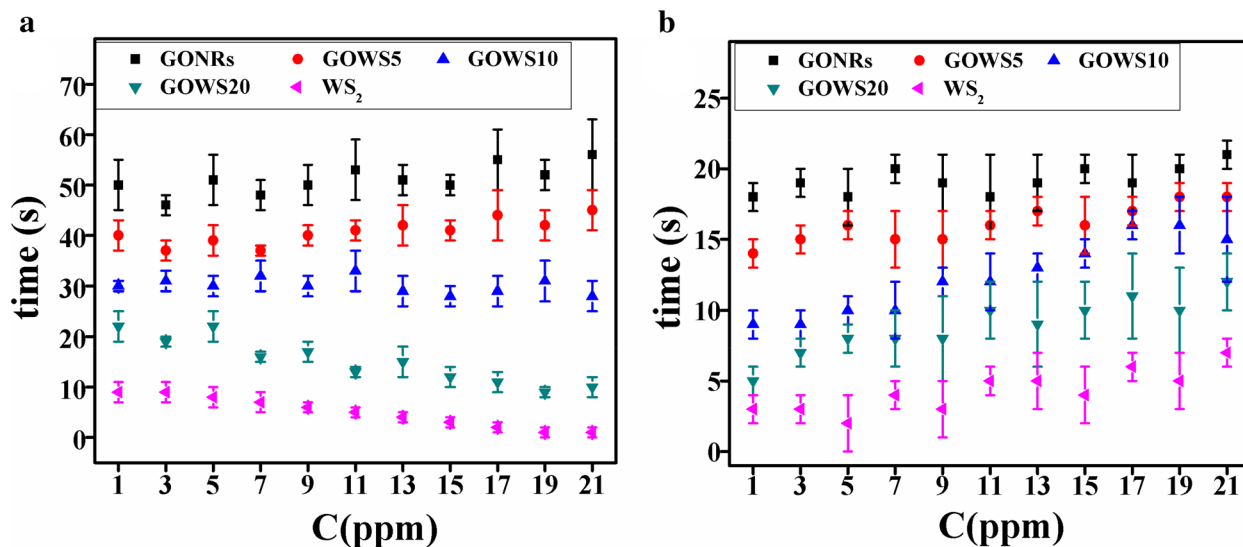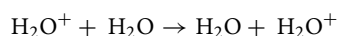
Figure 6. Response (**a**) and recovery (**b**) times of the samples versus ethanol concentration.

the closest physisorbed molecules on WS_2 flakes. The proton hopping through hydrogen bond networks could be explained as:

$$H_2O^+ + H_2O \rightarrow H_2O + H_2O^+$$

Since a higher gas response for WS_2 sheets was expected if they were electrically connected, GONRs were used to enhance the electrical conductivity. In fact, GONRs with high surface-to-volume ratio, abundant active edges and surface functional groups, is itself a sensitive material for physisorption of molecules[7,30]. Water and ethanol molecules interacted mainly with hydroxyl/carboxyl groups and form hydrogen bond networks[31,32]. In p-type GONR samples seems that the formation of hydrogen bond networks is the dominant mechanism due to the presence huge of GO surface functional groups, and improves the electrical current. So the gas response polarity is positive in p-type samples. It is noteworthy to mention that gradual penetration of the molecules through the graphene oxide inter-layers may results in hydrolyzing the inter-layer functional groups and enhances the ionic conductivity in one hand[33,34] however, it increases the response times on the other hand. Higher response in the present of the gas mixtures is due to the addition of ethanol–water hydrogen bonds to water–water hydrogen bonds[35–37]. In GOWS hybrid structure, the graphene oxide nanoribbons not only improved the connectivity of WS_2 nanoflakes but also provided p–n heterojunctions at the interface of p-type GONRs and n-type WS_2. So, the charge transfer mechanism may reduce the width of the depletion layer at the interfaces of p–n heterojunctions, which is a synergic effect as can be observed in Fig. 5b. The response and recovery times were also investigated as two key factors and the results are shown in Fig. 6a,b, respectively. As mentioned previously, water penetration and desorption are slow process in the case of GONRs which leads to higher response and recovery times in the samples with more values of GONRs along with less variation by increasing the ethanol concentrations. The response and recovery times were about 50 and 20 s for GONRs, and about 28 and 14 s for GOWS10, respectively at 15 ppm of ethanol@40% R.H., while were less than 10 s for WS_2 samples.

The fast reversibility of WS_2 may be due to the intrinsic hydrophobic nature of WS_2[27] and the large radius of tungsten element that facilitated desorption of gas molecules[26,38]. In the sensor with highest WS_2 content (i.e. GOWS20), lowest response and recovery times were observed which may be attributed to its high electrical resistance (~ 20 MΩ). Gas selectivity of GOWS10 was measured toward other available gases i.e. H_2, acetone, dry air, Argon and CO_2 at room temperature, shown in Fig. 7a, but there was no notable response compared to ethanol and humidity that could be due to the lack of hydrogen bond networks or negligible charge transfer exposed to non-polar or less polar molecules. The response value was about 3 and 10 for dray air and 100 ppm of acetone, while it was 113 and 240 for 40% R.H. and 11 ppm of ethanol @ 40% R., respectively.

To further investigate the role of relative humidity in sensor performance, ethanol response was measured in different relative humidity values. The results have compared in Fig. 7b for 5, 11, 15 and 21 ppm of ethanol in 20%, 40% and 70% R.H. For example, the obtained value was 60 for 20% relative humidity and was 90 for 5 ppm of ethanol @ 20% R.H., respectively. As the relative humidity enhanced up to 70%, the response increased linearly, could be resulting of hydrogen bond networks enhancement. The flexibility of GOWS10 sensor was also studied as an optimized sample coated on Kapton substrate including Au interdigitated electrodes under bending radius of 1 cm. The dynamic response curves of the bent sensor toward 5 ppm of ethanol@40% R.H. are shown in Fig. 7c. As can be clearly seen, before bending (i.e. in the flat mode), the response of sensor was about 149 while upon bending condition it decreased to about 137.5. The response and recovery times increased to 38 and 24 s respectively and the sensor response values decreased less than 8% in the first bending. After 10th bending cycle, the response values further decreased (~ 2.5%) and the response and recovery times increased to about 43 and 29 s respectively. Figure 7d displays the response values for 10th, 20th, and 30th bending cycles.
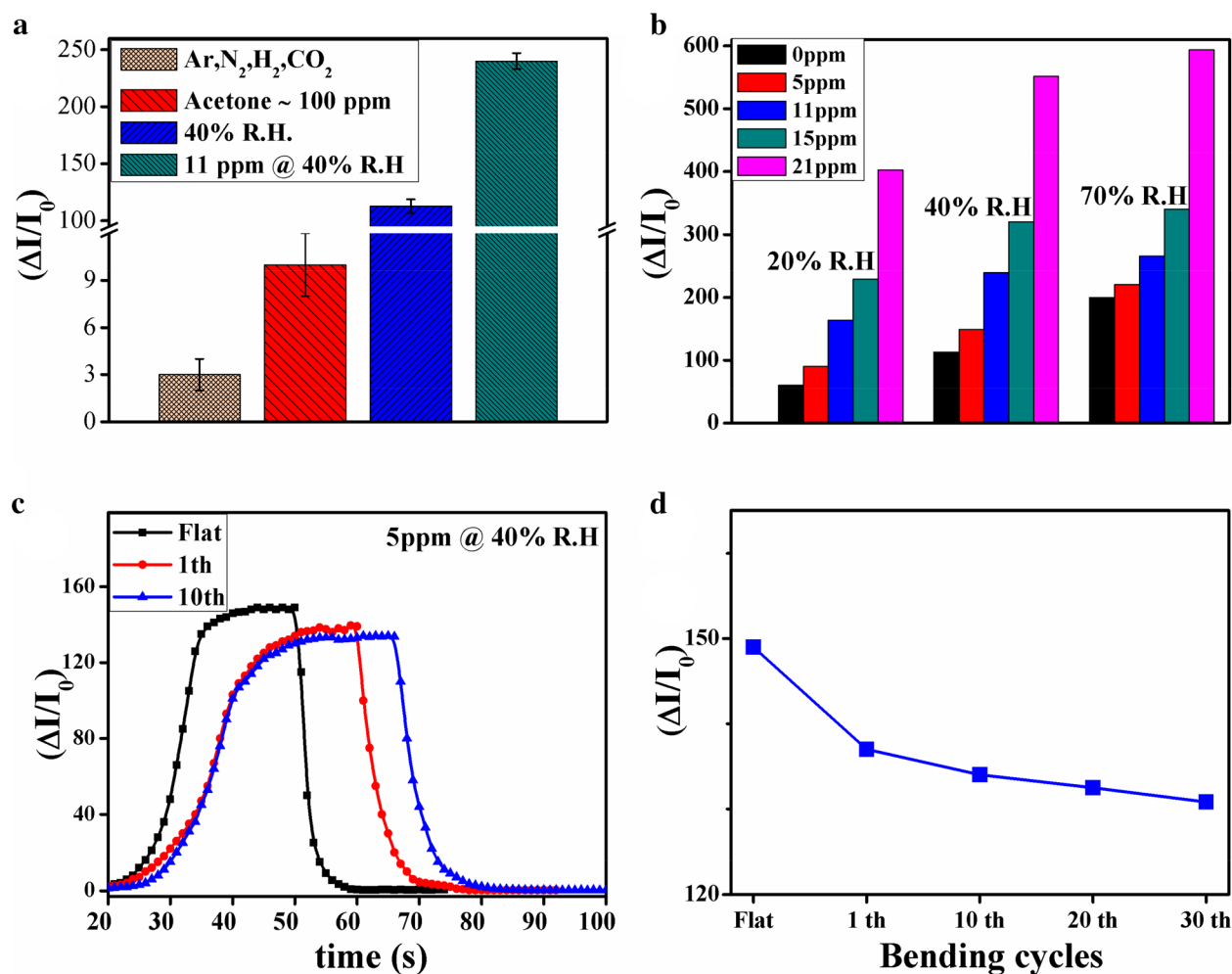
Figure 7. Responses of GOWS10 samples toward H_2, acetone, dry air (N_2), Argon, CO_2, 40% humidity and 11 ppm of ethanol at room temperature (**a**), response values for 5, 11, 15, and 21 ppm of ethanol in mixture of different R.H. (**b**), dynamic response curves of the bent sensors at 5 ppm of ethanol@40% R.H. (**c**), response values for 10th, 20th, and 30th bending cycles test (**d**).

Materials	EtOH (ppm)	Response	Working temperature (°C)	References
SnO_2@MoS_2	500	160	280	[42]
ZnO@Graphene	10	8.5	~400	[43]
SnO_2/Graphene	600	38.58	27	[44]
rGO/SnO_2	50	28.7	170	[45]
PVP/TiS_2	18	68	RT	[46]
WS_2/GONRs	1 21	13.5 438.5	RT RT	This work

Table 1. A summary of ethanol vapor sensing materials based on 2D nanostructures. *EtOH* ethanol vapor concentration, *RT* room temperature.

As indicated by the results, the response values, response and recovery times did not show significant changes after 10th bending cycle which turns the proposed sensor to a potential candidate for flexible applications. A summary of the proposed ethanol sensing platforms based on two dimensional composite nanostructures is listed in Table 1 and their results, regarding to detection limit, response value and working temperature as the most important characteristics, are compared with those obtained in the present study.

Methods

Preparation of WS₂ powder. WS_2 crystals were synthesized by CVT method without employing any transport agent at near atmosphere pressure (100 mbar). In this work, commercial mixed elements; tungsten and sulfur powders (from Merck Ltd., 99/99%) in stoichiometric proportions were located at one end of an evacuated
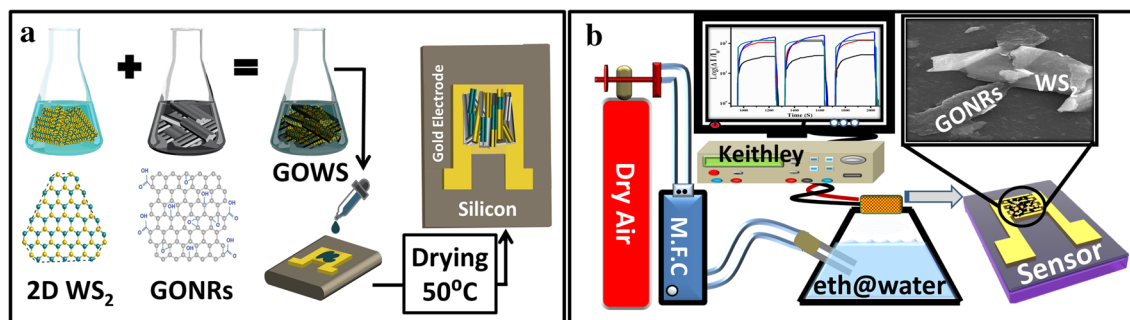
Figure 8. Schematic illustration of mixing process of WS$_2$ and GONRs as GOWS hybrid nanostructures and drop-casting method (**a**), schematic representation of ethanol sensing setup (**b**).

quartz ampule with 20 mm diameter, and length of about 150 mm. The sealed ampule was inserted in a tube furnace for about 8 days before encapsulation at room temperature. This mixture was heated at $T_{hot} = 1,323$ K ($\Delta T/t = 20$ C/min) whereas the other end of the ampule was at lower temperature $T_{cold} = 1,123$ K. Prior to powder insertion, the quartz ampule was cleaned with piranha, then was rinsed with DI-water and dried at 100 °C to remove contamination.

Preparation of GONRs.   Graphene oxide nanoribbons were synthesized through longitudinal unzipping of MWCNTs[19]. Briefly, 72 mL of H$_2$SO$_4$ was added to 300 mg MWCNTs in a round bottom flask and stirred for 1 h. Then, 8 mL of phosphoric acid (H$_3$PO$_4$ 85%) was added to the mixture and allowed to stir for another 15 min before the addition of KMnO$_4$ (2.4 g). The reaction mixture was transferred to an oil bath and heated at 65 °C for 2 h until a brownish suspension is obtained. After cooling to room temperature, the solution was poured onto 100 mL of iced DI water containing 10 mL H$_2$O$_2$ (30%). The resulting light brown colored graphene oxide nanoribbons (GONRs) precipitate was collected by centrifugation (13,000 rpm). Subsequently, the product was washed with DI-water several times until a neutral pH level was achieved.

Preparation of 2D hybrid nanostructures of WS$_2$/GONRs (GOWS).   The synthesized WS$_2$ powder was dispersed in 10 mL of ethanol and sonicated for 3 h at room temperature in order to exfoliate WS$_2$ flakes[39,40]. To prepare GOWS hybrid nanostructures and form WS$_2$/GONRs heterojunctions two solutions were mixed by using a magnetic stirrer for 1 h and sonicated for 24 h at room temperature[12]. Schematic of GOWS hybrid nanocomposite preparation and drop-casting on the substrate containing gold interdigitated electrodes is shown in Fig. 8a. The molar ratio of WS$_2$/GONRs (= X) was set to different values and the samples were named as GOWSX with X = 1, 5, 10,15and 20.

Sensor fabrication.   The ethanol sensing properties of GOWS samples were studied and compared with pristine WS$_2$, and GONRs. The sensors were fabricated by drop-casting 40 μL of each solution on a SiO$_2$ substrate, including sputtered gold interdigitated electrodes with an interspacing of 100 μm and an active area of 10 mm × 10 mm. After dropping, the substrates spin coated at 250 rpm to form a uniform film, following by drying at 50 °C for 20 min. The flexibility of GOWS was investigated on Kapton substrate with a bending radius of 1 cm.

Ethanol sensing setup.   Ethanol vapor sensing properties of the samples were measured in a breath simulator setup at room temperature. In this setup, the ethanol concentration was controlled by mixing different volume ratios of ethanol (from Merck Ltd., 99/9%) and DI-water (> 18 MOhm-cm). Ethanol vapor was generated by controlling the appropriate inlet dry-air flow to the mixed solution. The ethanol concentration was calculated according to Henry's law, from 1 to 21 ppm[41]. I–V measurement was performed using Keithely series 6487 Picoammeter as schematically shown in Fig. 8b.

Summary

Room temperature and high response ethanol and humidity sensors were prepared based on 2D hybrid nanostructures of WS$_2$/GONRs by a simple drop-casting method. Morphological and structural analysis of the as-prepared samples verified the formation of heterojunction structures between WS$_2$ and GONRs. The GONRs improved electrical connections between WS$_2$ nanosheets and the produced p–n junctions upgraded gas response of GOWS hybrid nanostructures. The sensing performance of GOWS was investigated with different molar ratio of WS$_2$ to GONRs and GOWS10 exhibited the highest response. The fast performance was observed for GOWS20 sample with response and recovery times of 22 and 5 s at 1 ppm of ethanol@40% R.H. Selectivity of GOWS was studied toward H$_2$, Argon, CO, and N$_2$ molecules. The flexibility tests were performed based on GOWS10 films on Kapton substrate with bending radius of 1 cm and the results revealed promising potentials for GOWS hybrid nanostructures in wearable sensors applications.

Data availability

Derived data supporting the findings of this study are available from the corresponding authors on reasonable request.

References

1. Jia, C., Batterman, S. & Godwin, C. VOCs in industrial, urban and suburban neighborhoods, Part 1: Indoor and outdoor concentrations, variation, and risk drivers. *Atmos. Environ.* **42**, 2083–2100 (2008).
2. Log, T. & Moi, A. Ethanol and methanol burn risks in the home environment. *Int. J. Environ. Res. Public Health* **15**, 2379 (2018).
3. Juang, D.-F., Lee, C.-H., Chen, W.-C. & Yuan, C.-S. Do the VOCs that evaporate from a heavily polluted river threaten the health of riparian residents?. *Sci. Total Environ.* **408**, 4524–4531 (2010).
4. Lachenmeier, D. W. Safety evaluation of topical applications of ethanol on the skin and inside the oral cavity. *J. Occup. Med. Toxicol.* **3**, 26 (2008).
5. Liu, X., Ma, T., Pinna, N. & Zhang, J. Two-dimensional nanostructured materials for gas sensing. *Adv. Funct. Mater.* **27**, 1702168 (2017).
6. Neri, G. Thin 2D: The new dimensionality in gas sensing. *Chemosensors* **5**, 21 (2017).
7. Donarelli, M. & Ottaviano, L. 2D materials for gas sensing applications: A review on graphene oxide, MoS_2, WS_2 and phosphorene. *Sensors* **18**, 3638 (2018).
8. Zhu, X., Guo, Y., Ren, H., Gao, C. & Zhou, Y. Enhancing the NO_2 gas sensing properties of rGO/SnO_2 nanocomposite films by using microporous substrates. *Sens. Actuators B Chem.* **248**, 560–570 (2017).
9. Zhou, Y., Gao, C. & Guo, Y. UV assisted ultrasensitive trace NO_2 gas sensing based on few-layer MoS_2 nanosheet–ZnO nanowire heterojunctions at room temperature. *J. Mater. Chem. A* **6**, 10286–10296 (2018).
10. Liu, G.-B., Xiao, D., Yao, Y., Xu, X. & Yao, W. Electronic structures and theoretical modelling of two-dimensional group-VIB transition metal dichalcogenides. *Chem. Soc. Rev.* **44**, 2643–2663 (2015).
11. Zhou, Y., Liu, G., Zhu, X. & Guo, Y. Ultrasensitive NO_2 gas sensing based on rGO/MoS_2 nanocomposite film at low temperature. *Sens. Actuators B Chem.* **251**, 280–290 (2017).
12. Park, S. Y. *et al.* Highly selective and sensitive chemoresistive humidity sensors based on rGO/MoS_2 van der Waals composites. *J. Mater. Chem. A* **6**, 5016–5024 (2018).
13. Yao, J. D., Zheng, Z. Q., Shao, J. M. & Yang, G. W. Stable, highly-responsive and broadband photodetection based on large-area multilayered WS_2 films grown by pulsed-laser deposition. *Nanoscale* **7**, 14974–14981 (2015).
14. Zhang, X., Wang, J., Xu, H., Tan, H. & Ye, X. Preparation and tribological properties of WS_2 hexagonal nanoplates and nanoflowers. *Nanomaterials* **9**, 840 (2019).
15. Toda, K., Furue, R. & Hayami, S. Recent progress in applications of graphene oxide for gas sensing: A review. *Anal. Chim. Acta* **878**, 43–53 (2015).
16. Huang, B. *et al.* Adsorption of gas molecules on graphene nanoribbons and its implication for nanoscale molecule sensor. *J. Phys. Chem. C* **112**, 13442–13446 (2008).
17. Modtland, B. J., Navarro-Moratalla, E., Ji, X., Baldo, M. & Kong, J. Monolayer tungsten disulfide (WS_2) via chlorine-driven chemical vapor transport. *Small* **13**, 1701232 (2017).
18. Hu, D. *et al.* Two-dimensional semiconductors grown by chemical vapor transport. *Angew. Chem. Int. Ed.* **56**, 3611–3615 (2017).
19. Higginbotham, A. L., Kosynkin, D. V., Sinitskii, A., Sun, Z. & Tour, J. M. Lower-defect graphene oxide nanoribbons from multi-walled carbon nanotubes. *ACS Nano* **4**, 2059–2069 (2010).
20. Chen, M. *et al.* Novel synthesis of NiS/MMT/GO nanocomposites with enhanced peroxidase-like activity for sensitive colorimetric detection of glutathione in solution. *Adv. Compos. Hybrid Mater.* **1**, 612–623 (2018).
21. Berkdemir, A. *et al.* Identification of individual and few layers of WS_2 using Raman Spectroscopy. *Sci. Rep.* **3**, 1755 (2013).
22. Nanda, S. S., Yi, D. K. & Kim, K. Study of antibacterial mechanism of graphene oxide using Raman spectroscopy. *Sci. Rep.* **6**, 28443 (2016).
23. Zeng, Y., Lin, S., Gu, D. & Li, X. Two-dimensional nanomaterials for gas sensing applications: The role of theoretical calculations. *Nanomaterials* **8**, 851 (2018).
24. Huo, N. *et al.* Photoresponsive and gas sensing field-effect transistors based on multilayer WS_2 nanoflakes. *Sci. Rep.* **4**, 5209 (2014).
25. Zhou, C. J., Yang, W. H., Wu, Y. P., Lin, W. & Zhu, H. L. Theoretical study of the interaction of electron donor and acceptor molecules with monolayer WS_2. *J. Phys. D Appl. Phys.* **48**, 285303 (2015).
26. Zhou, C., Yang, W. & Zhu, H. Mechanism of charge transfer and its impacts on Fermi-level pinning for gas molecules adsorbed on monolayer WS_2. *J. Chem. Phys.* **142**, 214704 (2015).
27. Jha, R. K. & Guha, P. K. Liquid exfoliated pristine WS_2 nanosheets for ultrasensitive and highly stable chemiresistive humidity sensors. *Nanotechnology* **27**, 475503 (2016).
28. Chen, Z. & Lu, C. Humidity sensors: A review of materials and mechanisms. *Sens. Lett.* **3**, 274–295 (2005).
29. Agmon, N. The Grotthuss mechanism. *Chem. Phys. Lett.* **244**, 456–462 (1995).
30. Lu, G., Ocola, L. E. & Chen, J. Reduced graphene oxide for room-temperature gas sensors. *Nanotechnology* **20**, 445502 (2009).
31. Bi, H. *et al.* Ultrahigh humidity sensitivity of graphene oxide. *Sci. Rep.* **3**, 2714 (2013).
32. Medhekar, N. V., Ramasubramaniam, A., Ruoff, R. S. & Shenoy, V. B. Hydrogen bond networks in graphene oxide composite paper: Structure and mechanical properties. *ACS Nano* **4**, 2300–2306 (2010).
33. DamascenoBorges, D., Woellner, C. F., Autreto, P. A. S. & Galvao, D. S. Insights on the mechanism of water-alcohol separation in multilayer graphene oxide membranes: Entropic versus enthalpic factors. *Carbon* **127**, 280–286 (2018).
34. Devanathan, R., Chase-Woods, D., Shin, Y. & Gotthold, D. W. Molecular dynamics simulations reveal that water diffusion between graphene oxide layers is slow. *Sci. Rep.* **6**, 29484 (2016).
35. Pothoczki, S., Pusztai, L. & Bakó, I. Variations of the hydrogen bonding and hydrogen-bonded network in ethanol–water mixtures on cooling. *J. Phys. Chem. B* **122**, 6790–6800 (2018).
36. Gereben, O. & Pusztai, L. Hydrogen bond connectivities in water–ethanol mixtures: On the influence of the H-bond definition. *J. Mol. Liq.* **220**, 836–841 (2016).
37. Stehle, S. & Braeuer, A. S. Hydrogen bond networks in binary mixtures of water and organic solvents. *J. Phys. Chem. B* **20**, 4425–4433 (2019).
38. Li, X., Li, X., Li, Z., Wang, J. & Zhang, J. WS_2 nanoflakes based selective ammonia sensors at room temperature. *Sens. Actuators B Chem.* **240**, 273–277 (2017).
39. Luo, S. *et al.* Rational and green synthesis of novel two-dimensional WS_2/MoS_2 heterojunction via direct exfoliation in ethanol-water targeting advanced visible-light-responsive photocatalytic performance. *J. Colloid Interface Sci.* **513**, 389–399 (2018).
40. Zhou, K.-G., Mao, N.-N., Wang, H.-X., Peng, Y. & Zhang, H.-L. A mixed-solvent strategy for efficient exfoliation of inorganic graphene analogues. *Angew. Chem. Int. Ed.* **50**, 10839–10842 (2011).

41. Sin, M. L. Y. *et al.* Ultralow-power alcohol vapor sensors using chemically functionalized multiwalled carbon nanotubes. *IEEE Trans. Nanotechnol.* **6**, 571–577 (2007).

42. Yan, H., Song, P., Zhang, S., Yang, Z. & Wang, Q. Dispersed SnO_2 nanoparticles on MoS_2 nanosheets for superior gas-sensing performances to ethanol. *RSC Adv.* **5**, 79593–79599 (2015).

43. Liang, S. *et al.* Deposition of cocoon-like ZnO on graphene sheets for improving gas-sensing properties to ethanol. *Appl. Surf. Sci.* **357**, 1593–1600 (2015).

44. Borude, R. R. *et al.* Facile synthesis of SnO_2 -graphene composites employing nonthermal plasma and SnO_2 nanoparticles-dispersed ethanol. *J. Phys. D Appl. Phys.* **52**, 175301 (2019).

45. Xu, S. *et al.* Reduced graphene oxide-based ordered macroporous films on a curved surface: General fabrication and application in gas sensors. *ACS Appl. Mater. Interfaces.* **8**, 3428–3437 (2016).

46. Hosseini-Shokouh, S. H., Fardindoost, S. & Zad, A. I. A High-performance and low-cost ethanol vapor sensor based on a TiS_2/PVP composite. *ChemistrySelect* **4**, 6662–6666 (2019).

Acknowledgements

Author contributions

H.A., A.I., and R.M. wrote the main manuscript text, and analyzed the gas sensing data. The sensing diagrams, material synthesis, and gas sensing measurements were performed in collaboration with H.A. and S.H.H.S., who also helped the discussion part of gas sensing mechanisms. The GONRs were synthesized by E.A. All authors reviewed the manuscript and commented on different parts.

Competing interests

The authors declare no competing interests.

Additional information

Correspondence and requests for materials should be addressed to A.I. or R.M.

Reprints and permissions information is available at www.nature.com/reprints.

Publisher's note Springer Nature remains neutral with regard to jurisdictional claims in published maps and institutional affiliations.